

Deliverable D3.1: VNA MMW/THz measurements and calibration essays using TERAmeasure head

Date of issue: 28-Dec-2021

Due date: 31-Dec-2021

Document Ref: TERAmeasure_D_3.1_Anritsu_v1.2

Leader in charge of deliverable: ANRITSU

Dissemination level		
PU	Public	X
PP	Restricted to other program participants (including the Commission Services)	
RE	Restricted to a group specified by the consortium (including the Commission Services)	
CO	Confidential, only for members of the consortium (including the Commission Services)	



This project has received funding from the European Union's research and innovation program under Grant Agreement No. 862788 (TERAmeasure).

Document updates

Version	Date	Author	Organisation	Changes
0.1	10/12/2021	Daniel Gallego	UC3M	Initial version
0.2	21/12/2021	Daniel Gallego	UC3M	Updated figures
1.0	22/12/2021	Guillermo Carpintero	UC3M	Executive summary and Introduction sections
1.1	23/12/2021	Guillermo Carpintero	UC3M	Content of Section 4
1.2	27/12/2021	Jon Martens	ANRITSU	Full revision and text edits

Abbreviations

CPS	Co-Planar Stripe	EDFA	Erbium-doped optical fiber amplifier
CPW	Co-Planar Waveguide	GHz	Gigahertz (10E9)
DUT	Device under test	MMW	Millimeter-wave frequency range
ΔL	S21 additional attenuation	PC	Polarization controller
ΔZ	Elevation offset	PCA	Photo-Conductive Antenna
ΔX	Lateral offset	RF	Radiofrequency
ΔY	Axial offset	THz	Terahertz frequency range
$\Delta\alpha$	Yaw offset	TSA	Tapered Slot Antenna
$\Delta\beta$	Pitch offset	VNA	Vector Network Analyzer
		W1	1.0 mm coaxial connector standard

Statement of independence

The work described in this document is genuinely a result of efforts pertaining to the TERAmesure project. Any external source is properly referenced

Confirmation by Authors:

Daniel Gallego, UC3M
Guillermo Carpintero, UC3M
Jon Martens, ANRITSU

Table of Contents

1. Executive Summary	4
2. Introduction	6
3. TERAmeasure photonic-driven RF probe heads	8
4. TERAmeasure W1-driven RF probe heads	14
4.1 Introduction.....	15
4.2 Test Structures	15
4.3 TERAmeasure non-contact probing assessment.....	17
5. Summary and Conclusion	26
Annex 1: TERAmeasure probing measurements raw data	28

Page in blank intentionally

1. Executive Summary

According to the grant agreement, the objective of this deliverable is to provide “information regarding the first evaluation of the probe heads interfaced to Vector Network Analyzer for frequency response measurements”. The main objective of this report is to provide public information about the measurements and calibration studies of TERAmesure RF probe heads after the assembly process that confirm the successful assembly of the probe heads and the feasibility of the novel probing concept.

Within the project, we have structured the activities around two key developments, each one enabling us to demonstrate the successful achievement of two TERAmesure key breakthroughs independently:

- a) the development of a W1-driven RF probe heads, and
- b) the development of a photonic-driven RF probe heads.

The first one, based on developing a 1.0 mm connector W1-driven probe heads, aims to develop TERAmesure non-contact probe concept using dielectric waveguides. As a project de-risk strategy, we have developed RF probes which interface with current Vector Network Analyzer (VNA) equipment using standard 1.0 mm connectors. This approach enables us to connect the probe to the available ANRITSU VNA and evaluate the non-contact probing concept performance.

The second one, based on developing a photonic-driven probe heads, aims to develop a photonic-based Radio-Frequency signal generation system in the probe, benefiting from the ultrawide bandwidth of photonics to unlock an operating frequency range from 30 GHz to 3 THz.

This deliverable presents the results achieved within these two key developments:

- For the W1-driven probe heads, we present results on the non-contact probe, characterizing the landing interconnection using the available ANRITSU VNA.
- For the photonic driven probes, we present basic measurements on samples mounted with Photo-Conductive Antenna (PCA) photomixers, showing parameters such as dark current and photocurrent, which allow assessing the success of the probe assembly.

Page in blank intentionally

2. Introduction

TERAmeasure project main objective is to develop a novel non-contact millimetre (MMW, 30 GHz -300 GHz) and Terahertz (THz, 300 GHz – 3 THz) frequency measurement paradigm for instrumentation and sensing unlocking metrology-grade results. To achieve this goal, the project has developed **non-contact RF probe heads** that operate over the MMW and THz range, and this deliverable presents the first measurements and calibration studies using the novel TERAmeasure RF probe heads.

The development of TERAmeasure RF probe heads has been organized in two main activities, each enabling us to demonstrate a TERAmeasure key breakthrough, independently.

The first activity is linked to TERAmeasure key breakthrough KB1, to **unlock continuous-wave frequency generation and phase sensitive detection** over the entire MMW and THz wave ranges, integrating a 1550 nm photomixing emitter (Tx) and receiver (Rx) with wideband antennas, using photonics-based Radio-Frequency generation, through microwave photonics techniques to generate RF signals continuously over the MMW and THz bands. This activity has been to develop a **photonic-driven RF probe**, which aims to develop a photonic-based Radio-Frequency signal generation system in the probe, benefiting from the ultrawide bandwidth of photonics to unlock an operating frequency range from 30 GHz to 3 THz.

The second activity is linked to TERAmeasure key breakthrough KB2, unlock lensing structures within dielectric waveguides to maximize the near-field coupling efficiency in the MMW/THz range. The probe interface is a standard 1-mm connector, which enables us to connect this probe to current Vector Network Analyzer equipment, **to evaluate the non-contact probing concept**. This activity appeared as a de-risk strategy, aiming to develop a **W1-driven RF probe head** to demonstrate TERAmeasure novel non-contact probe concept using dielectric waveguides for the wideband interconnect

According to the grant agreement, the objective of this deliverable is to provide “information regarding the first evaluation of the probe heads interfaced to Vector Network Analyzer for frequency response measurements”. The main objective of this report is to provide public information about the measurements and calibration essays of TERAmeasure RF probe heads after the assembly process, aiming to confirm the successful assembly of the RF probe heads and the feasibility of the novel probing concept.

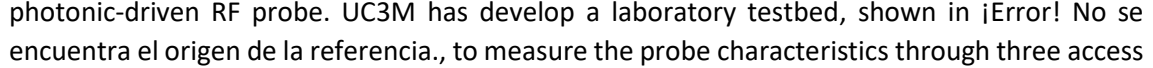
In the following sections we provide the results achieved for the measurements and calibration studies within these two activities:

- For the **photonic-driven RF probe**, we present basic measurements on samples mounted with Photo-Conductive Antenna (PCA) photomixers, showing parameters such as dark current and photocurrent, which allow assessing the success of the probe assembly.
- For the **W1-driven RF probe head**, we present results on the non-contact probe, characterizing the landing interconnection using the available ANRITSU VNA, which prove the success of the novel concept for non-contact probing.

Page in blank intentionally

3. TERAmeasure photonic-driven RF probe heads.

Within this section, we report the measurements and calibration studies with the **photonic-driven RF probe**. This RF probe, designed at UC3M, includes a novel structure of an Indium Phosphide (InP) Photo-Conductive Antenna (PCA) photomixer, fabricated at Fraunhofer HHI, specifically designed to couple with the novel concept for non-contact probing, fabricated on silicon at KTH.

The assembly process of all these elements took place at UC3M, producing the first sample of a photonic-driven RF probe. UC3M has developed a laboratory testbed, shown in  Error! No se encuentra el origen de la referencia., to measure the probe characteristics through three access ports:

- a) A **fiber-optic access port**, to inject an optical signal onto the PCA active area,
- b) A **coaxial access port**, to bias the PCA, and collect the photocurrent,
- c) A **dielectric-waveguide access port**, which is the high frequency interconnect port for the probing.

With this setup, we have been able to measure key parameters to assess the PCA performance after the assembly process, such as the dark current (PCA photocurrent without any light input at the fiber access port) and the generated photocurrent level (PCA photocurrent at different optical input power levels at the fiber access port) at different bias voltages.

The assembled photonic driven RF probe was assessed in the laboratory testbed setup. We were able to measure either the generated dark current and photocurrent, what demonstrate a successful assembly process. Below we present and discuss the results obtained from these measurements.

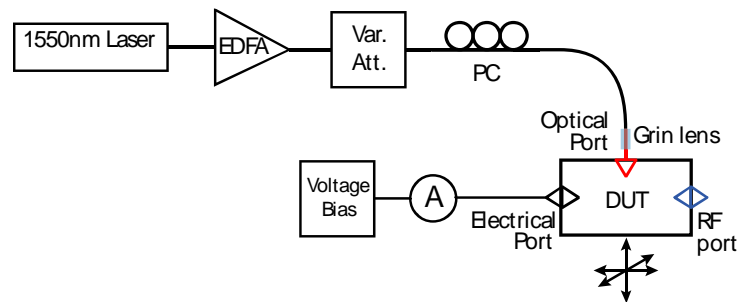
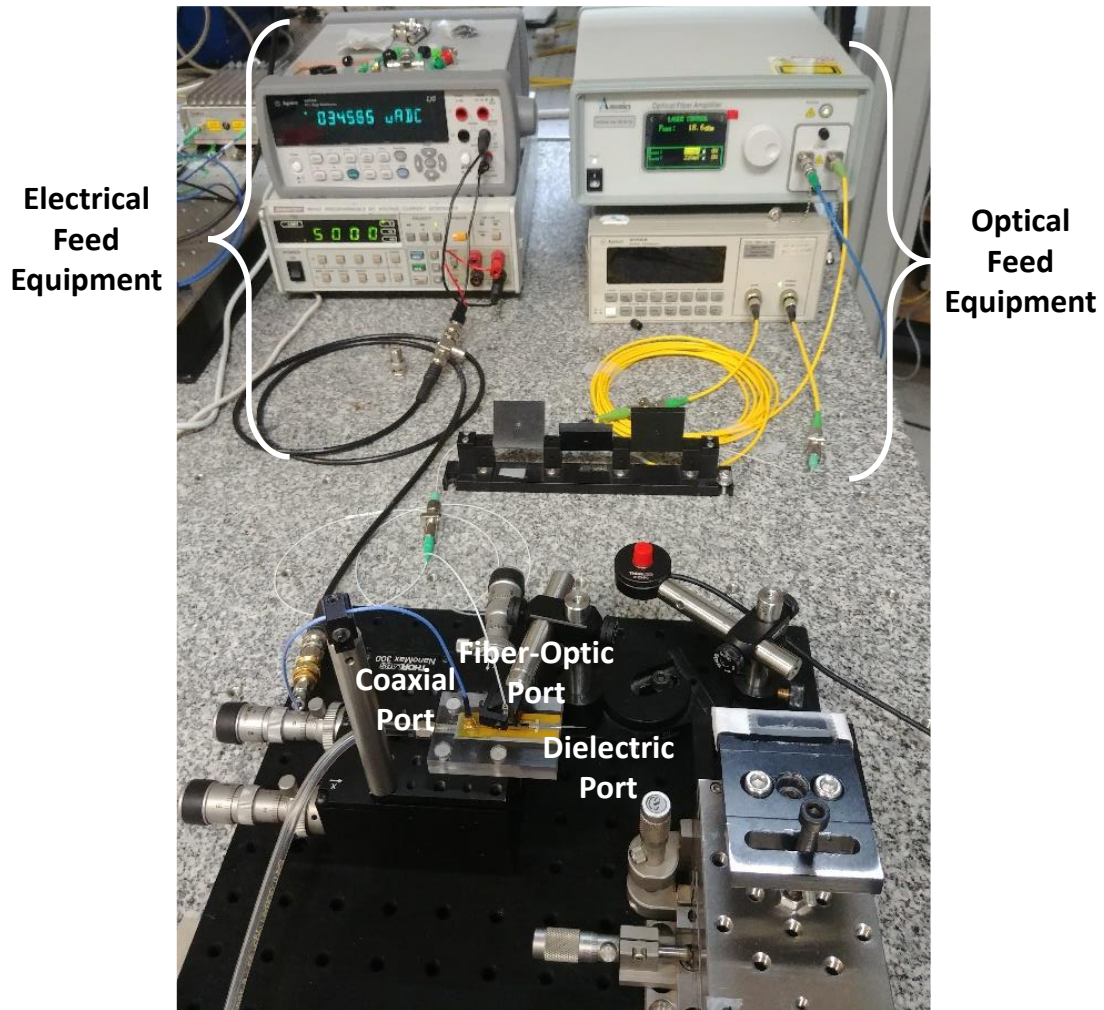


Figure 3-1. Photocurrent characterization setup photograph and scheme. A constant voltage power supply is used to bias the PCA of the device under test (DUT) whereas an ammeter (A) is monitoring the current. The dark current is measured in dark illumination condition (absence of incident light on the PCA). To measure the sensitivity (photocurrent versus incident optical power) curves at different bias voltage, the light from a 1550 nm tuneable diode laser is amplified using an EDFA and attenuated with a precision optical variable attenuator (Var. Att.) to illuminate the PCA with optical power in the range from 0 to 30 mW. The output power at the output of the grin lens at the different attenuation levels was measured using a power meter before and after the photocurrent measurements to ensure good accuracy. The optical power is focused in a spot of approximately 10 μm on the PCA using a 1:1 grin lens. The DUT is mounted in a 3D translational stage to achieve optimal optical coupling. The generated photocurrent is measured using the ammeter for different optical power and bias voltage. The polarization state of the incident light is adjusted via a polarization controller (PC) to maximize the photocurrent generated. The bias voltage is increased in 50mV steps until reaching the non-linear regime of the PCA. The bias voltage is not further increased to avoid the damage of the DUT.

The measured dark current (Figure 3-2 top, blue line) was around 7 μA at a bias voltage of 0.5 V. The obtained dark current was much higher compared with the expected one for an unmounted PCA (around 0.4 μA @ 0.5V). This suggest there was a lower impedance path for the current in the probe compare to the resistance of the PCA ($> 1 \text{ M}\Omega$). That was confirmed afterward measuring a resistance of 76.2 $\text{k}\Omega$ between the TSA antenna pads on silicon (Figure 3-3). Taking into account this resistance in parallel with the PCA, we finally estimate a darkcurrent of 0.44 μA @ 0.5V. The effect of this lower resistance path on the dielectric waveguide port have not been addressed yet and is going to be included in new simulations.

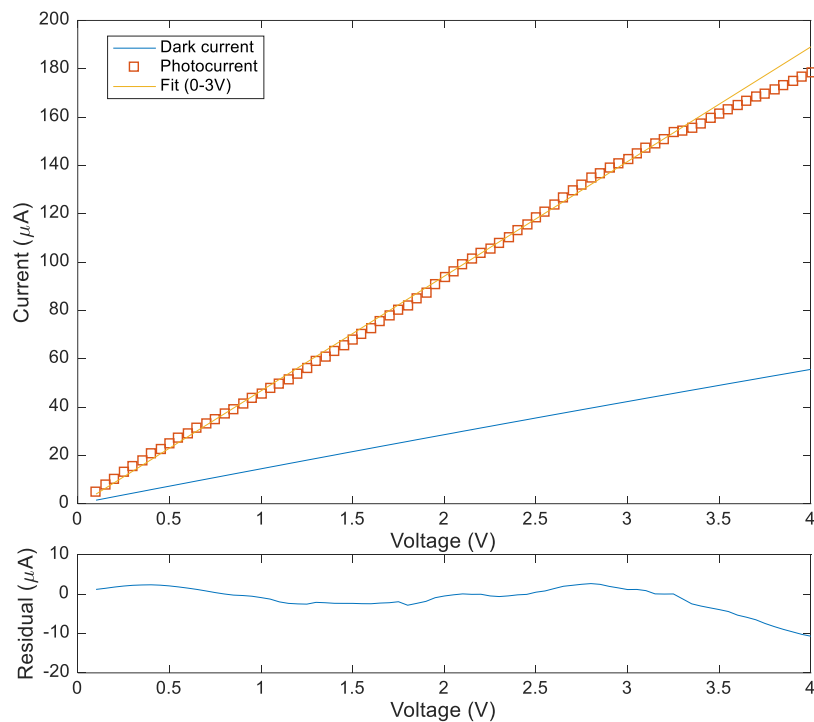


Figure 3-2. (Top) Dark current and photocurrent generated by 30 mW CW optical power versus bias voltage. The linear regression fit of the data from 0 up to 2 V is shown as well. (Bottom) Residual of measurement data and linear regression fit.

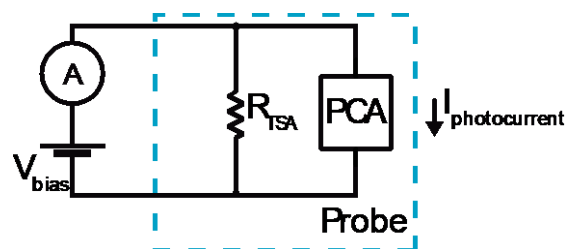


Figure 3-3. Dark Current leakage path inside the probe. R_{TSA} is equal to 76.2 $\text{k}\Omega$, the resistance measured between the pads of the TSA antenna on silicon.

The photocurrent is obtained subtracting the dark current from the current measured when some optical power reaches the PCA. The photocurrent obtained for an incident optical power of 30 mW for different bias voltage in steps of 50 mV is shown in Figure 3-3 top (square trace). The voltage bias was increased until some deviation from linearity was observed. A linear regression fit of the data points below 2V (orange trace) shows that at 3.5 V the change of the

photocurrent with the bias voltage starts to diminish as can be seen from the residual plot at the bottom of Figure 3-2.

In order to obtain the sensitivity, the ratio between the generated photocurrent and the incident optical power, photocurrent curves were measured for different optical power at constant voltage, inside the linear range, in steps of 0.1V from -1 to 1 V (Figure 3-4). As we can see the PCA has the same sensitivity no matter the polarity of the bias voltage. The sensitivity obtained for each voltage is the slope of the corresponding curve. The sensitivity changes linearly with the bias voltage as it is shown in Figure 3-5. From a linear fit it is obtained that the sensitivity is $1.71 \cdot V$ mA/W. This value can be considered valid up to 3.5V where the device starts to show non linearities.

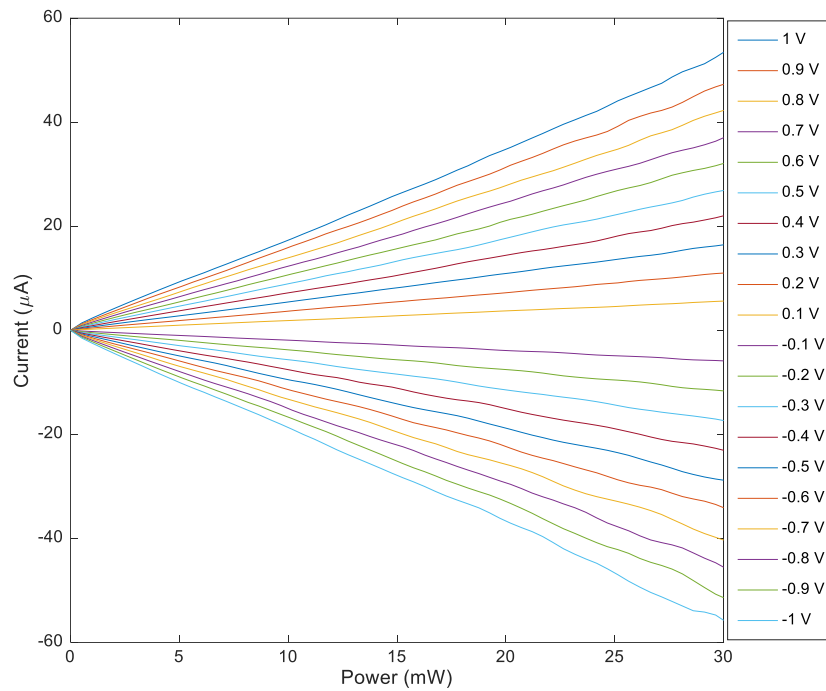


Figure 3-4. Photocurrent generated versus optical power for different bias voltage.

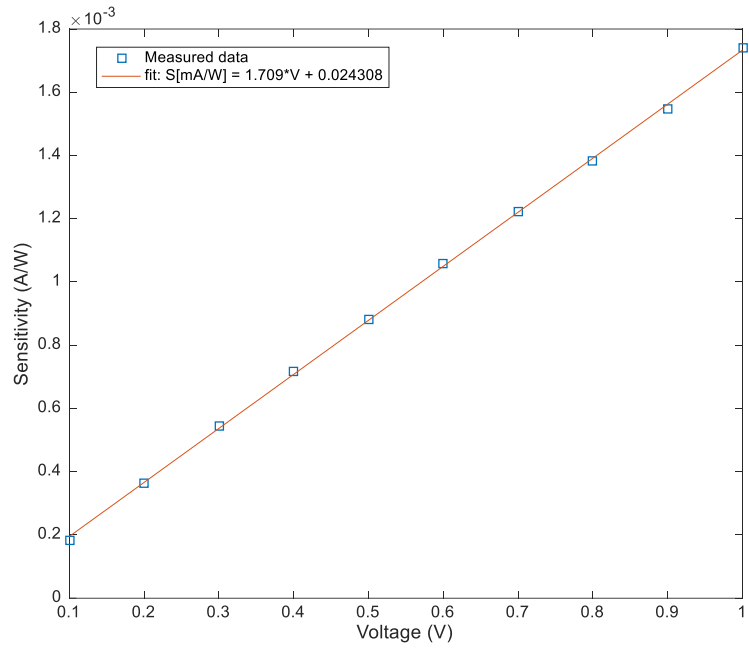


Figure 3-5. PCA sensitivity vs voltage.

Summarizing, with this set of measurements we demonstrate that the assembly procedure of the TERAmesure photonic-driven RF probe heads was a success. The PCA was correctly mounted on the head: there was electrical connection and the photocurrent was measured. The linear response of the photocurrent implies that the PCA was not damaged during the assembly. The high dark current measured comes from the relative low resistance of the silicon wafer where the TSA antennas are on top. Further simulations will be required to study the impact of this resistance in the reception high frequency signals.

Page in blank intentionally

4. TERAmesure W1-driven RF probe heads.

4.1 Introduction

Within this section, we report the measurements and calibration studies with the **W1-driven RF probe heads**. This RF probe, designed at UC3M, was proposed as a de-risk strategy in Deliverable 1.1 for the photonic-driven probe, based on powerful reasons:

- 1) Developing a RF probe sample using TERAmesure novel dielectric waveguide structure, which can be attached to Anritsu MS4647B Vector Network Analyzer equipped with Anritsu 3743A millimeter-wave broadband extension heads (70 kHz to 110 GHz operating range), enables us to perform early tests of the near field coupling concept using a standard VNA system independently of the success of the novel photonic component development,
- 2) Developing and demonstrating non-contact probing using a commercial ANRITSU VNA, broadly known by the Radio-Frequency community, will provide TERAmesure novel probe concept trust from this community,
- 3) Opens current VNA owners with coaxial interfaces into a customer base of TERAmesure probes. If we demonstrate that **W1-driven RF probe heads** can also interface with a variety of standard rectangular waveguide flanges, it will further increase the number of potential users for these probes.

The concept and design of the W1-driven RF probe head was done at UC3M, using a commercially available PCB launch 1.0 mm female connector (DC-110 GHz) and a specifically designed dielectric waveguide fabricated on silicon at KTH, mounted on a Rogers substrate provided by UC3M.

4.2 Test Structures

To experimentally demonstrate the performance of the proposed high-frequency interconnect, we assembled a back-to-back proof-of-concept of TERAmesure dielectric waveguide probe interconnection structure shown in **Figure 4-1**, using PCB launch 1.0 mm female connectors (DC-110 GHz) at the RF ports. The TERAmesure non-contact interconnect, described in European patent application EP20382960.1, uses a Tapered Slot Antenna (TSA) and a dielectric waveguide, requiring a Co-Planar Waveguide (CPW) to Co-Planar Stripe (CPS) transitions to enable feeding the TSAs from W1 1-mm coaxial connectors. A low permittivity material (Rogers RT/Duroid 5880) was used to fabricate the substrates on which the TSA antennas were defined, and the 1.0 mm connectors mounted. This enables us to experimentally measure the S parameters of the structure with an Anritsu MS4647B Vector Network Analyzer, equipped with Anritsu 3743A millimeter-wave broadband extension heads that enable measuring from 70 kHz to 110 GHz.

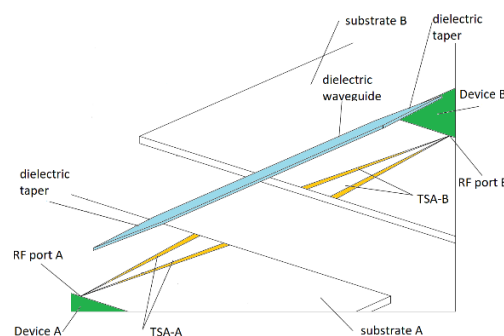


Figure 4-1: TERAmesure probe concept structure covering the millimeter- and Terahertz wave ranges of the spectrum based on combination of co-planar antennas (TSA-A and TSA-B) coupled through a dielectric waveguide (EU Patent pending).

In addition to the novel structure, to isolate the effects introduced by the W1 connectors and the CPW to CPS transitions, we have produced TestBoard-A0 and TestBoard-A test structures, fabricated as references. The measurement results of the different test boards are shown in **Figure 4-2**. The different test boards and the meaningfulness of the results are the following:

- **TestBoard-A0:** This test structure is used to assess the 1.0 mm connectors and their launches. Two W1-connectors are connected in a back-to-back configuration through a CPW line specified by the manufacturer. The manufacturer specified insertion losses are -0.489 dB at 10 GHz, -2.693 dB at 90 GHz and -7.117 at 110 GHz with a Rogers RO3003 substrate. The measurements with this structure are shown in light blue line on **Figure 4-2**. Given the back-to-back configuration, our results agree with the manufacturer data.
- **TestBoard-A:** This test structure is used to assess the effects of introducing the required CPW-to-CPS transition. The measurements with this structure are shown in dark blue line on **Figure 4-2**, show no significant deviations from the TestBoard-A0 trace. This allows us to conclude that the transition does not significantly alter the results.
- **TestBoard-B:** This is the first test structure including TERAmesure dielectric waveguide probe interconnection concept. It is used to evaluate the dielectric interconnection, where the two RF ports are interconnected using TERAmesure TSA and dielectric waveguide pair, in which the two TSA antennas are defined on a common substrate. **Figure 4-2** shows in dark brown the response without the dielectric waveguide (“TestBoard-B (without Rod)”) which compares with the result including the dielectric waveguide between the TSAs (“TestBoard-B (CPW-CPS-Rod)”), with the light brown trace.
- **TestBoard-C:** This test structure includes TERAmesure dielectric waveguide probe interconnection concept and is used to evaluate the effect of having the two RF ports in different substrates. The black trace (“TestBoard-C (CPW-CPS-Rod-Gap)”) shows that there is no appreciable degradation with respect to the single substrate case (“TestBoard-B (CPW-CPS-Rod)”). This is an important demonstration of the ability to use the probing technology in a practical setup.

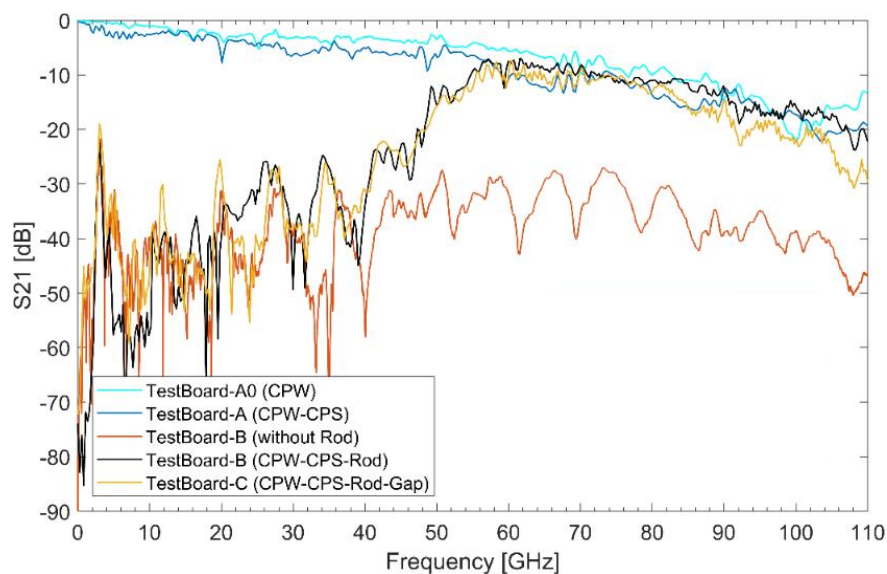


Figure 4-2: Measured transmission coefficients (S21) of the different test board structures, feed by W1-coaxial connectors

The main conclusion is that TERAmessure dielectric waveguide probe interconnection structure behaves as expected. It presents a low cut-off frequency, determined by the dielectric waveguide design. From this cut-off, which in the above demonstration was set at 50 GHz, **TERAmessure interconnection does not add any penalty to the standard CPW interconnect**. The high-frequency response shown in **Figure 4-2** is solely determined by the commercial 1.0 mm connectors.

4.3 TERAmessure non-contact probing assessment

To test TERAmessure RF probe concept and determine the probe alignment tolerances, we use a pair of TestBoard-C substrates, as shown in **Figure 4-3**. Each one includes a W1-connector, followed by a CPW line, a CPW-to-CPS transition, and TSA antenna. Both are assembled separately, to obtain two identical units, which are placed on independent methacrylate base plates.

On one of them, we glue the dielectric waveguide, carefully placing it in its optimum position, symmetrically with respect to the TSA pads. This structure becomes **TERAmessure W1-driven RF probe head**.

The other one is left as mounted initially, including the W1-connector and Rogers RT/Duroid 5880 with the CPW line, CPW-to-CPS transition and the TSA antenna becoming **TERAmessure landing substrate**.

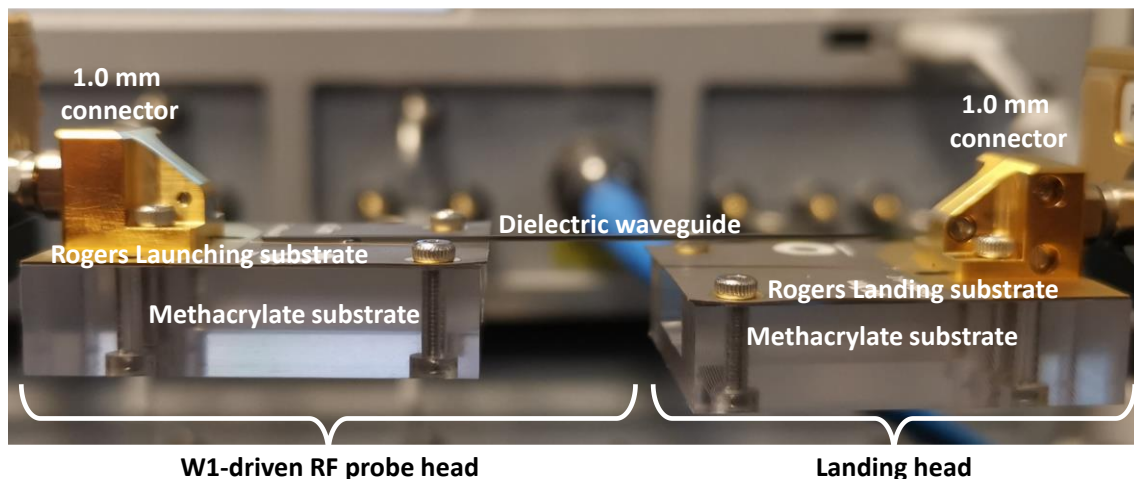


Figure 4-3: W1-driven RF probe head and landing substrate units, mounted on independent methacrylate base plates using TestBoard-C substrates.

With the **W1-driven RF probe head** and **landing substrate** assemblies, we now set up the experimental testbed. Its core is a two-port Anritsu MS4647B Vector Network Analyzer which include a pair of Anritsu 3743A Millimeter-Wave Modules. Both ports have a male 1 mm coaxial connector. Each broadband extension head was mounted on positioning stages, as shown in **Figure 4-4**, providing five degrees of freedom between the two structures. These allow us to analyze the alignment tolerances in five key degrees of freedom, shown in **Figure 4-5**, including the three coordinate axis ΔX (Lateral), ΔY (Axial), ΔZ (Elevation), and two angular axis, $\Delta\alpha$ (Yaw) and $\Delta\beta$ (Pitch). For every unit of displacement in each degree, the frequency is swept using 10.001 points, linearly distributed from 70 kHz to 110 GHz. The VNA intermediate frequency (IF) bandwidth is set to 1 kHz. Each frequency sweep takes 11 seconds.

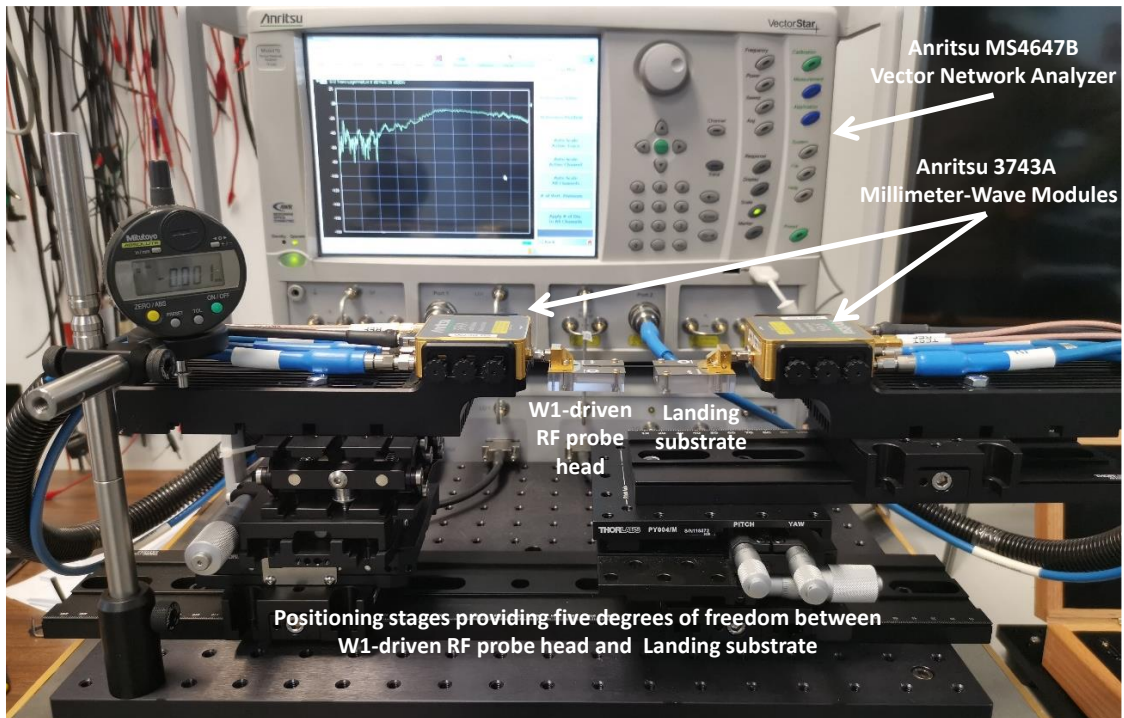


Figure 4-4: Alignment tolerance experimental setup. The structures were fixed through the W1-coaxial connectors to the Anritsu 3743A millimeter-wave broadband extension heads, which were placed onto positioning stages with five degrees of freedom.

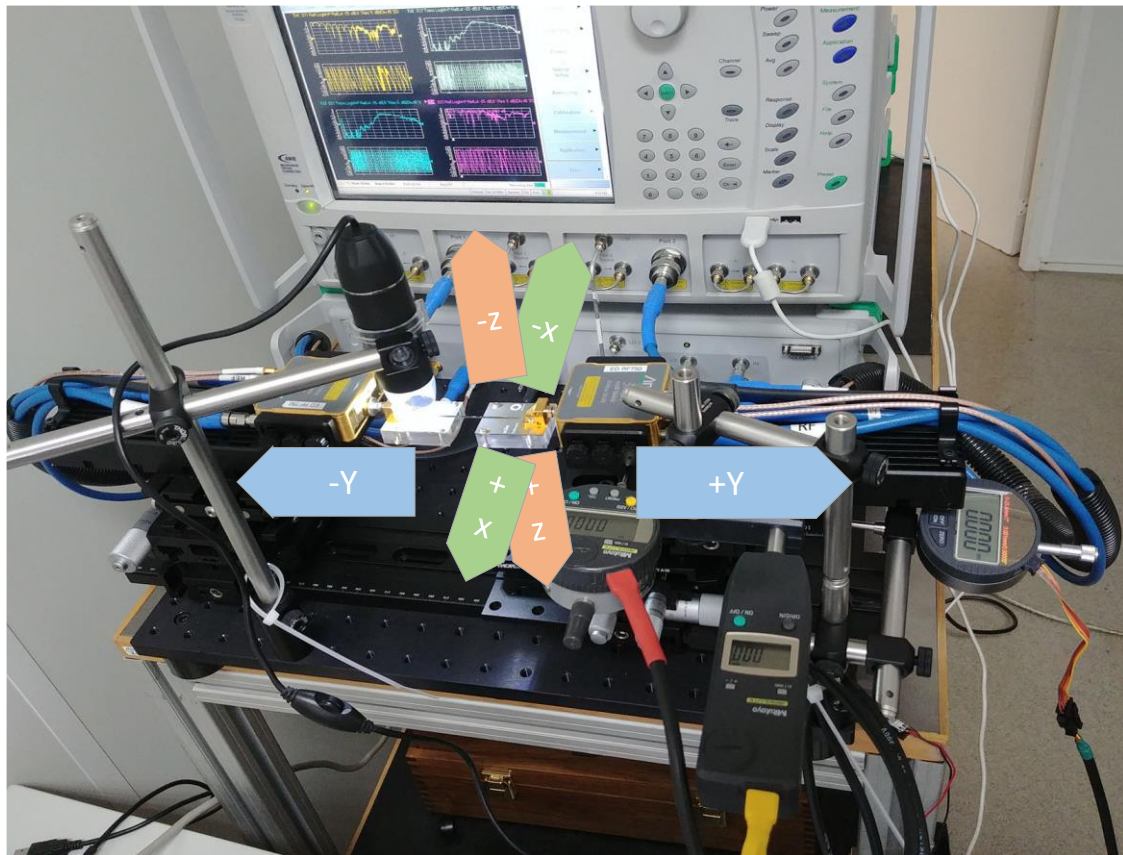


Figure 4-5. Degrees of freedom which are explored for probe alignment tolerance: Three coordinate axis, ΔX (Lateral), ΔY (Axial), ΔZ (Elevation), and two angular axes, $\Delta \alpha$ (Yaw) and $\Delta \beta$ (Pitch).

The S21 measurements over the full frequency range of the VNA, 70 kHz to 110 GHz, were performed when positions on each of the coordinate axis were varied. The results are shown from the low cutoff frequency that we found previously with the Test Structure (see section 4.2). The results are shown in the following figures: **Figure 4-6** for ΔZ (Elevation), **Figure 4-7** for ΔX (Lateral), **Figure 4-8** for ΔY (Axial), and for the two angular coordinates, $\Delta\alpha$ (Yaw) in **Figure 4-9** and $\Delta\beta$ (Pitch) in **Figure 4-10**.

The first graph for every coordinate axis shows the difference between the measured S21 parameter at a given offset value with respect to the S21 measured at the optimum position of the dielectric waveguide. The offsets for each coordinate axis (ΔX , ΔY , ΔZ , $\Delta\alpha$ and $\Delta\beta$) are given a positive sign when increase in the direction defined by the arrows of **Figure 4-5**, and the optimum position is determined by full-wave simulations of the back-to-back model, and is defined in terms of insertion losses, flatness of the S21 and maximum working frequency in a fundamental-mode working regime.

The graphs result in 2D maps, which plot the magnitude of S21(Offset, f) at different offset values minus the magnitude at the optimum location S21(Optimum, f) (in dB terms). Therefore, the maps represent the response as the additional attenuation, ΔL , introduced by the offset for each axis.

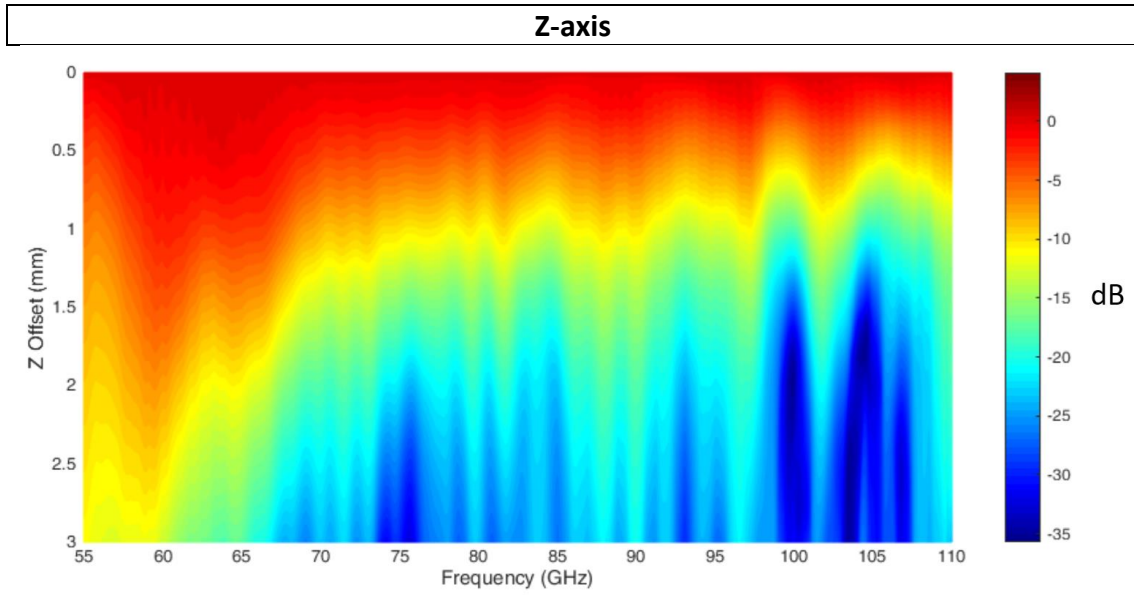
The measurements demonstrate that TERAmessure probing solution is extremely tolerant to spatial alignment errors:

- ΔZ (Elevation): The offset in this direction is positive when lifting the dielectric waveguide vertically from the substrate, and therefore can only have positive offsets, since we cannot push the dielectric waveguide through the substrate. The 2D map shown in **Figure 4-6(a)** demonstrates that the probe has a low cutoff frequency as we found previously with the Test Structure (see section 4.2). We have extracted for each frequency the elevation offset at which the response has dropped 1 dB, shown in **Figure 4-6(b)**, from which it is possible to ensure a connection loss lower than 1 dB for frequencies up to 110 GHz if the alignment error is smaller than 100 μm . For the sake of completeness, we have also obtained the elevation offset which produces a 15° phase change in the S21 response, shown in **Figure 4-6(c)**.
- ΔX (Lateral): In the X-axis, there are two directions in which we can move the dielectric waveguide. Looking from the dielectric waveguide towards the landing substrate TSA, to the right (+) and to the left (-). The 2D map is shown in **Figure 4-7(a)**, revealing that the signal goes through as long as the dielectric waveguide lies within the arms of the landing substrate TSA. **Figure 4-7(b)** and **Figure 4-7(c)** present the offset in each direction at which the response has dropped 1 dB and for which the phase changes 15° respectively. **Figure 4-7(b)** shows that an error of $\pm 700 \mu\text{m}$ around the optimum landing site still ensures a $\Delta L < 1 \text{ dB}$
- ΔY (Axial): The offset in this direction is positive when retreating backwards the dielectric waveguide from the tip of the TSA. Testing Y-offsets lower than -0.8 mm (moving the dielectric waveguide towards the 1.0 mm connector) were not possible in our setup since the DRW can damage the CPW-to-CPS transition. The 2D map shown in **Figure 4-8(a)** demonstrates that the probe is extremely tolerant in this direction with millimeter scale offsets.

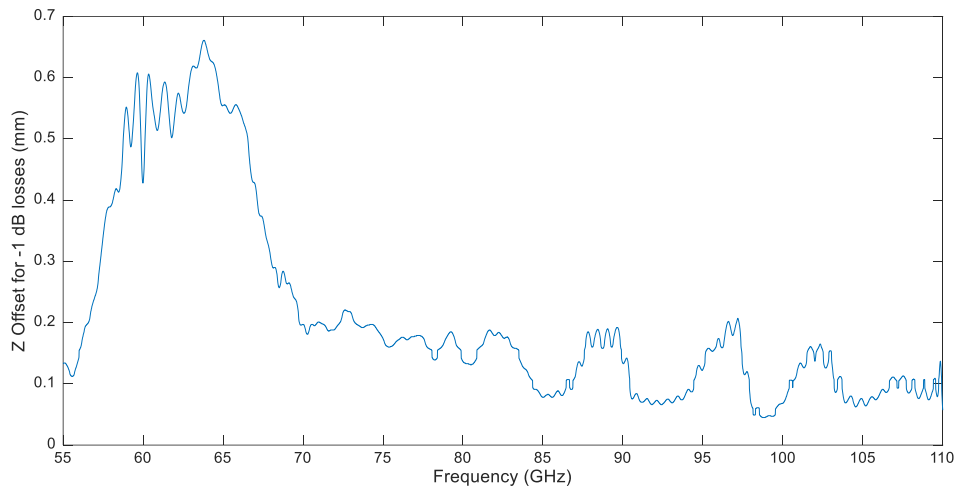
A key aspect from these measurements is that demonstrate the possibility to achieve efficient signal coupling without physical contact. A 40 μm gap between the dielectric waveguide probe and the landing substrate ensures a transmission loss $\Delta L < 1$ dB up to 110 GHz. If a $\Delta L < 3$ dB is acceptable, then a gap of 150 μm is allowed.

According to our study, the probe is robust to angular error. Up to 110 GHz, a yaw error (in-plane angular error, $\Delta\alpha$) smaller than $\pm 1.5^\circ$ allows achieving the $\Delta L < 1$ dB criterion. Due to limitations in our setup, the pitch angle study was bounded to 0.45° . A $\Delta L < 1$ dB was achieved for all angles and all frequencies up to 110 GHz. According to our simulations, the appearance of higher-order modes limits each axis and each angle tolerances for frequencies where a multi-mode regime is possible for the DRW, so a trade-off between maximum working frequency and mechanical precision can be set for a measurement setup. For this DRW design, special care must be placed when aligning the probe and the landing pad axes for frequencies above 200 GHz.

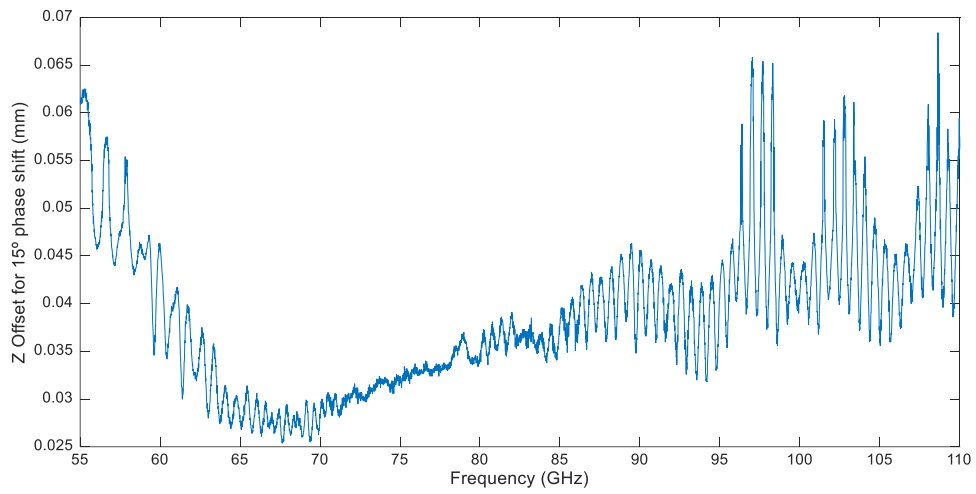
A tolerance study for frequencies above 110 GHz requires integrating optoelectronics sources and detectors in our system. The current status is that the assembly process has been successful, as reported in Section 3 of this document. The assessment of the functionality will be reported in Deliverable D1.5.



(a)



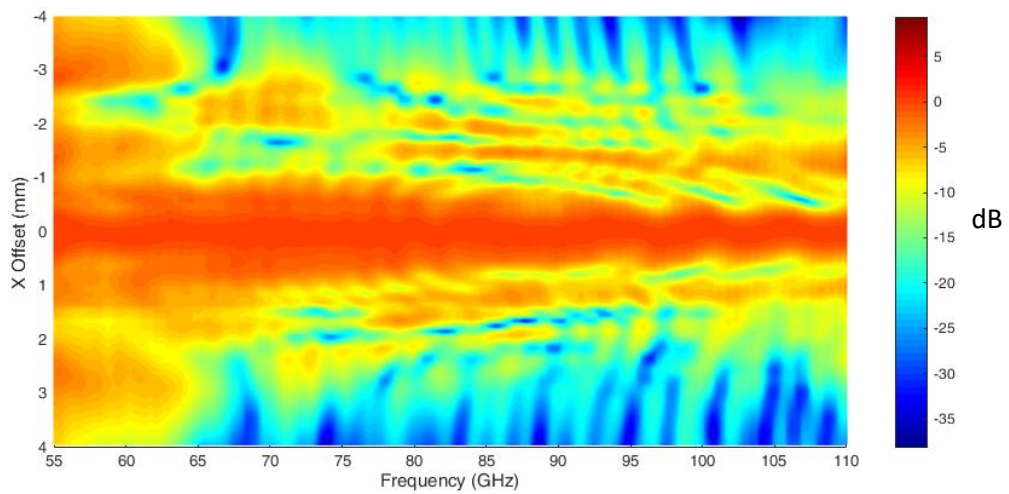
(b)



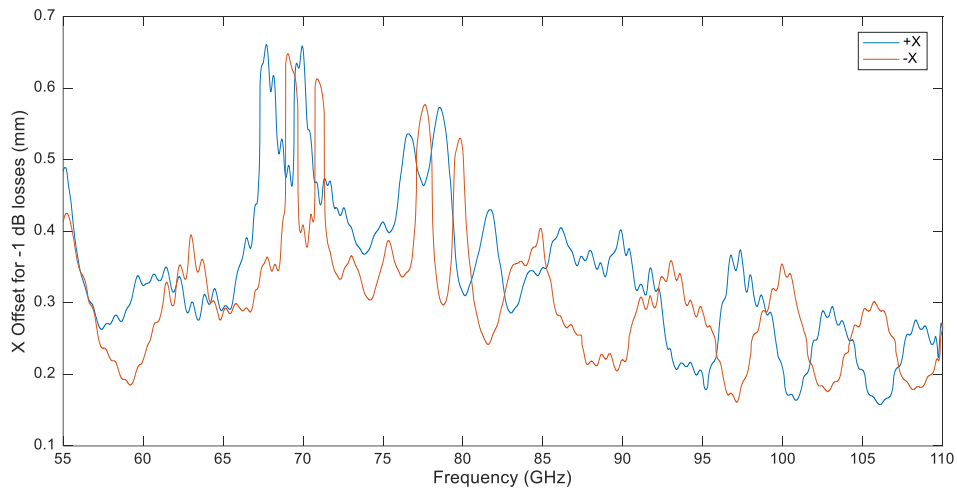
(c)

Figure 4-6. (a) Z-offset vs magnitude of $S_{21}(z,f)$ – Reference $S_{21}(f)$, (b) Z offset for 1 dB losses, and (c) Z offset for 15° phase shift.

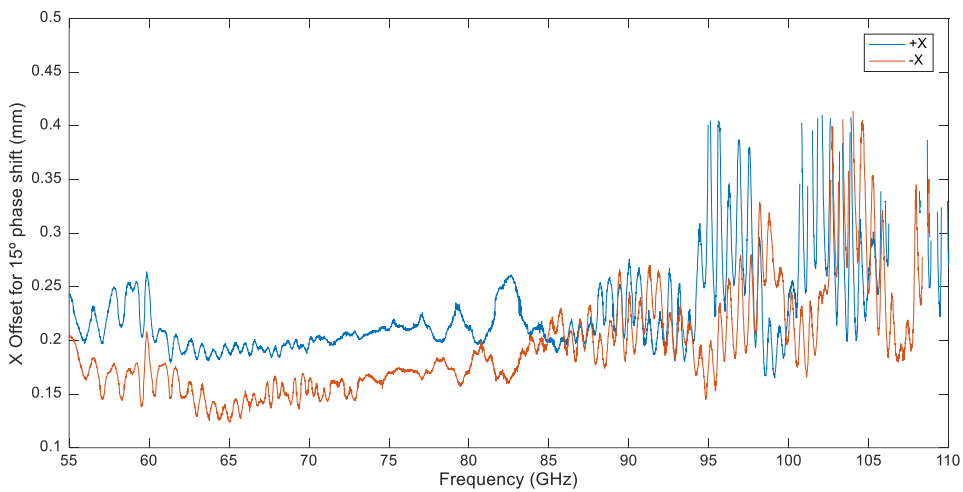
X-axis



(a)



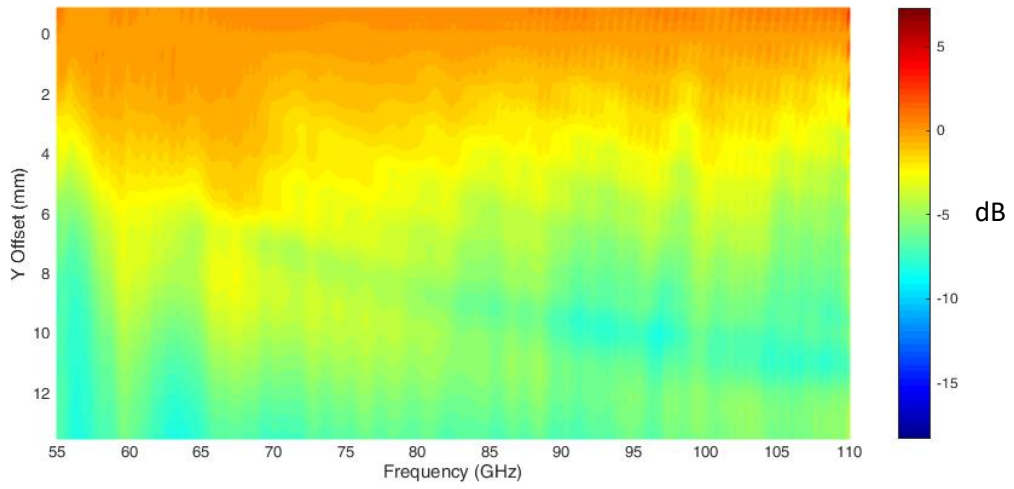
(b)



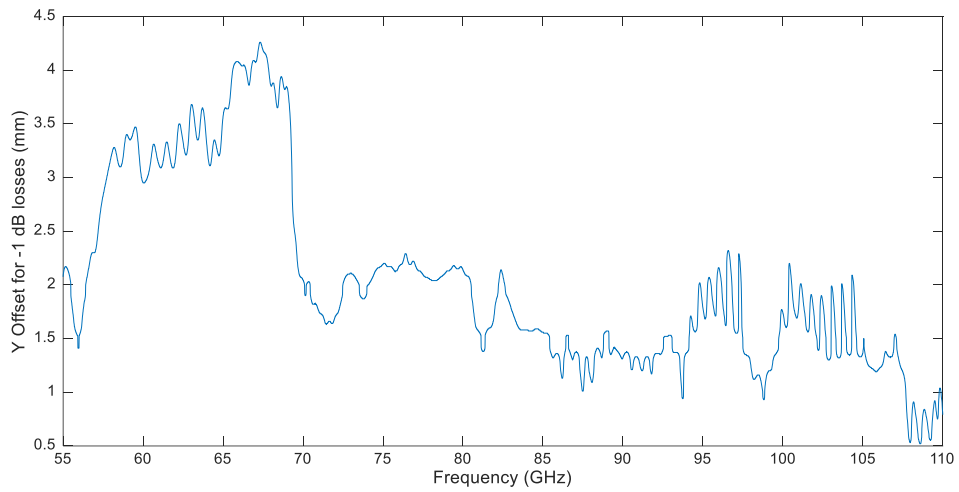
(c)

Figure 4-7. (a) X-offset vs magnitude of $S_{21}(z,f)$ – Reference $S_{21}(f)$, (b) +X and -X offset for 1 dB losses, and (c) +X and -X offset for 15° phase shift.

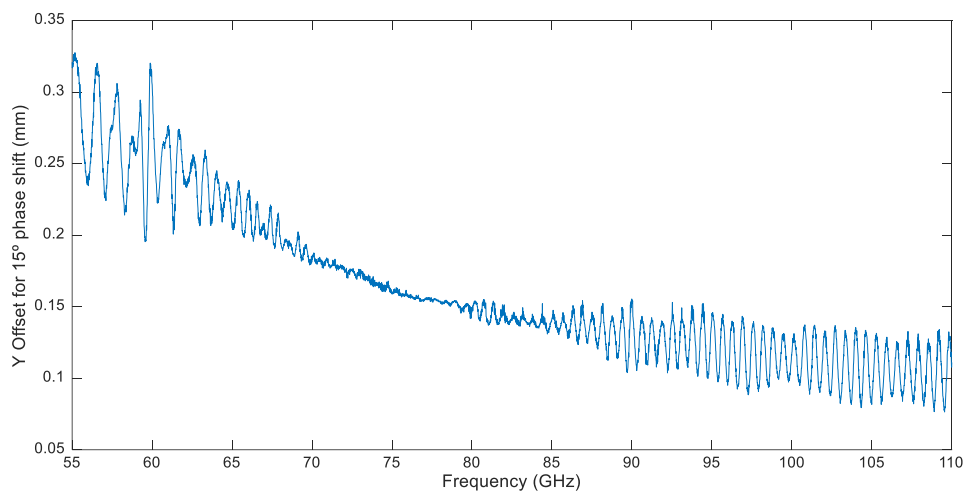
Y-axis



(a)



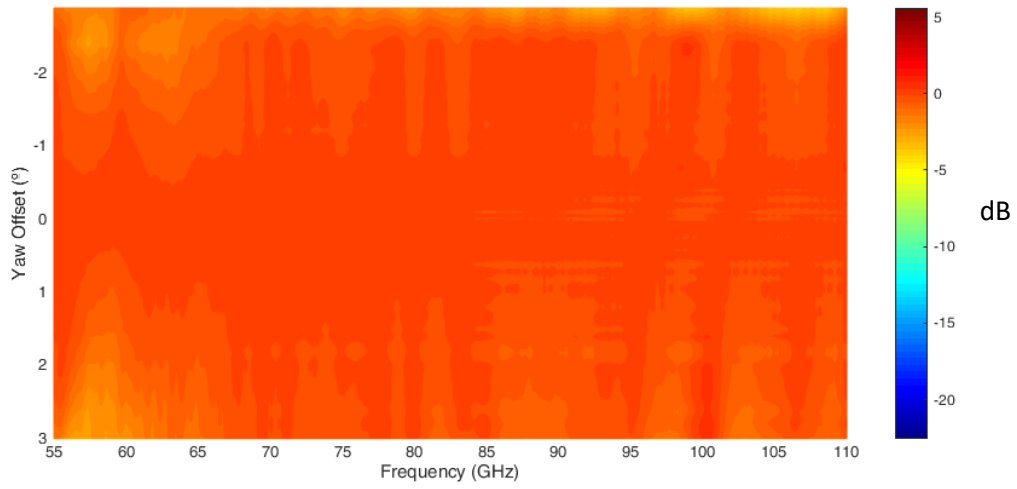
(b)



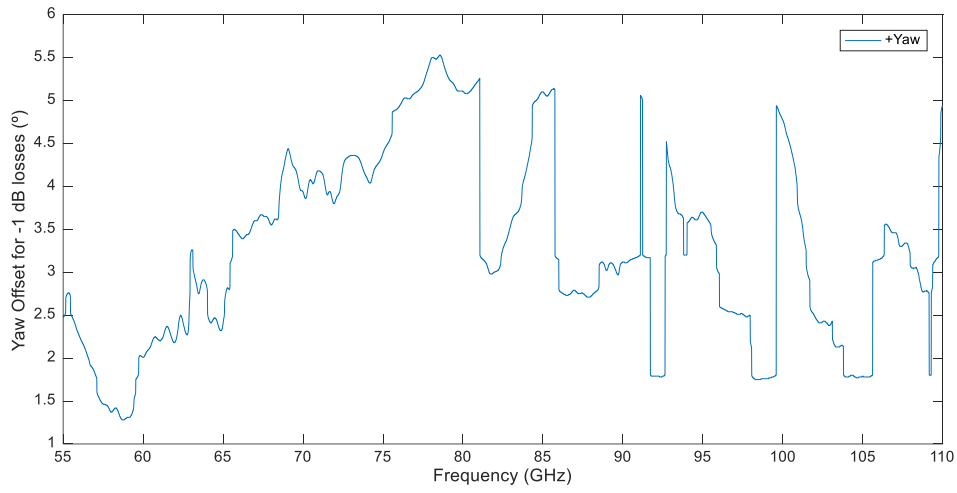
(c)

Figure 4-8. (a) Y-offset vs magnitude of $S_{21}(z,f)$ – Reference $S_{21}(f)$, (b) Y offset for 1 dB losses, and (c) Y offset for 15° phase shift.

Yaw-axis



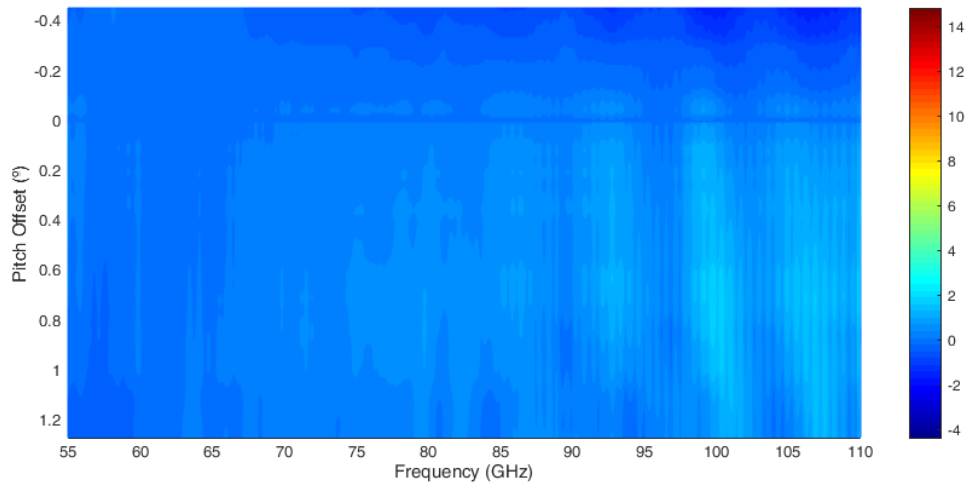
(a)



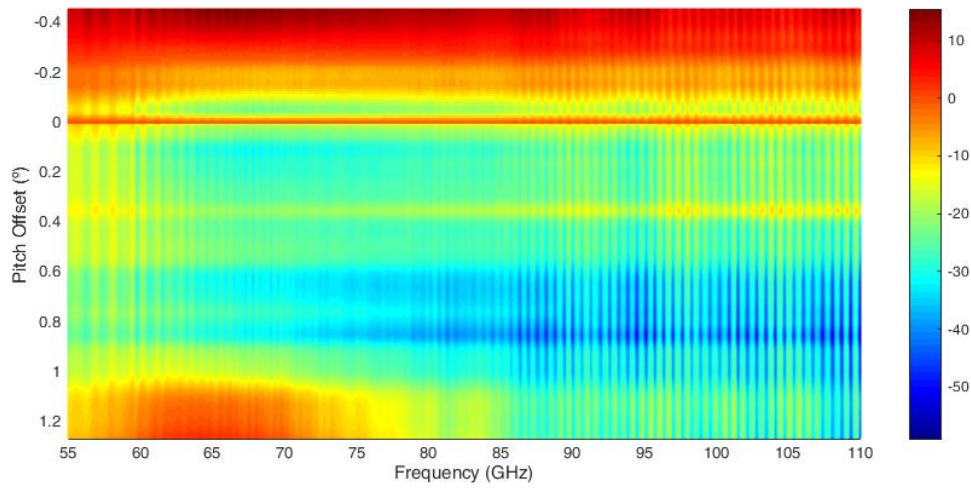
(b)

Figure 4-9. (a) Yaw-offset vs magnitude of $S_{21}(z,f)$ – Reference $S_{21}(f)$, (b) Yaw offset for 1 dB losses.

Pitch-axis



(a)



(b)

Figure 4-10. (a) Pitch-offset vs magnitude of $S_{21}(z,f) - \text{Reference } S_{21}(f)$, (b) Pitch-offset angle vs phase $S_{21}(\text{pitch},f) - \text{Reference } S_{21}(f)^*$.

Page in blank intentionally

5. Summary and Conclusion

Two prototypes of the radiofrequency test probe have been manufactured and characterized.

With the **photonic-driven RF probe** head we have validated the probe assembly process, to couple the novel Indium Phosphide Photoconductive (PCA) photomixer structure to the silicon launcher structure. We have measured the dark current and photocurrent of the probe and assessed the influence of the high resistive silicon in this assembly.

With the **W1-driven RF probe head**, we have validated the novel probing concept and demonstrated insertion losses ΔL smaller than 1 dB at 110 GHz within the tolerances of ± 100 μm in the X-axis, ± 700 μm in the Y-axis, a gap between probe and landing pad up to ± 40 μm , and error angles in the pitch and yaw of 0.45° and $\pm 1.5^\circ$ respectively.

A key advantage of this probe is that we have demonstrated that it is **backward compatible** with coaxial (up to the 1.0 mm connector) and rectangular waveguide interconnection standards.

Page in blank intentionally

Annex 1: TERAmesure probing measurements raw data.

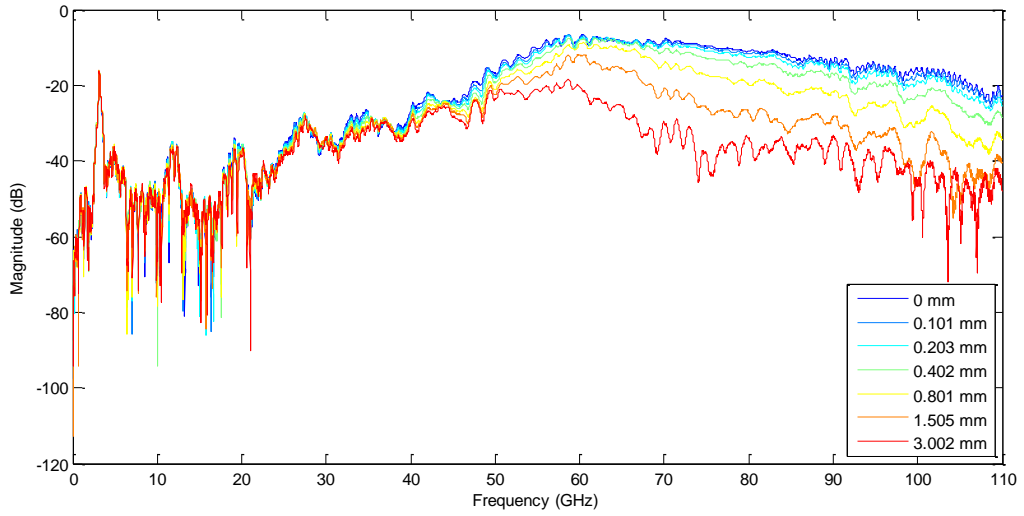


Figure A1-1. S21 at different z offset.

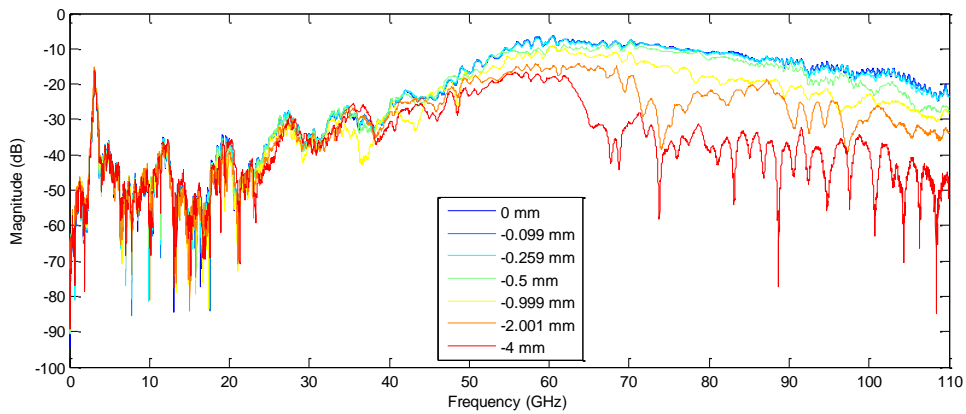
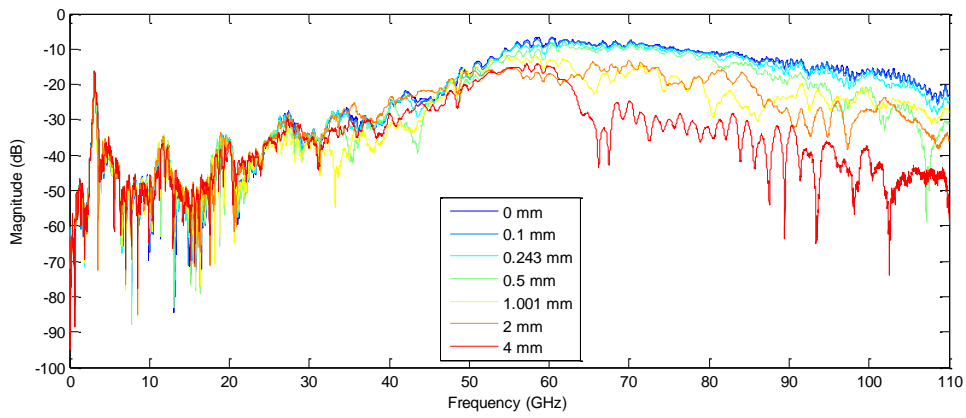


Figure A1-2. S21 at different +x and -x offsets.

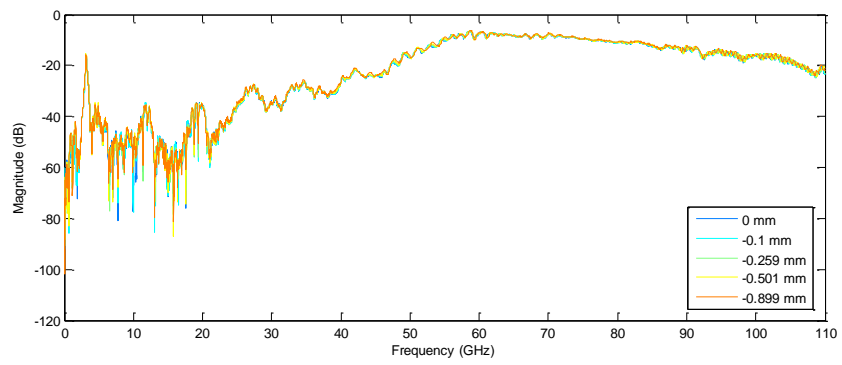
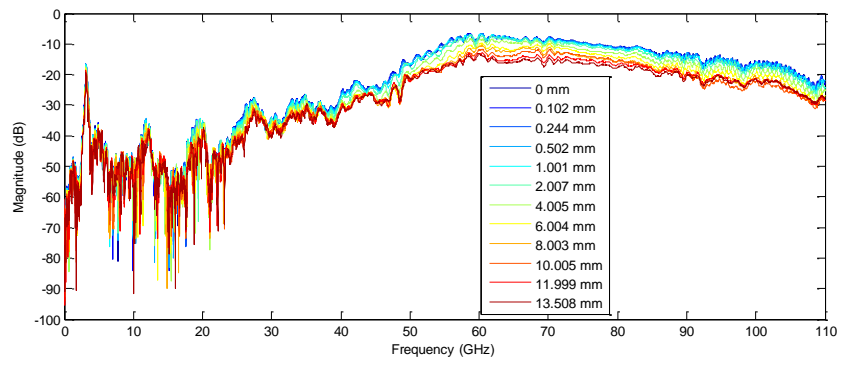


Figure A1-3. S21 at different y offset.

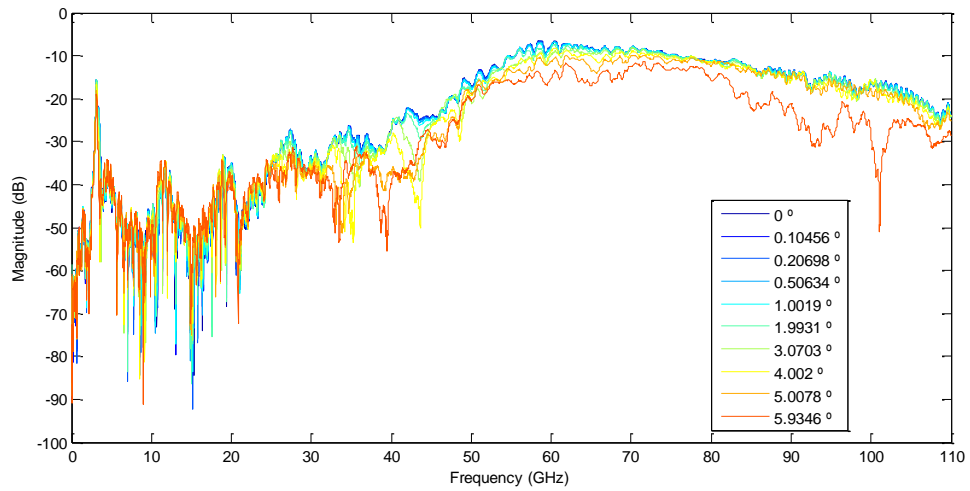
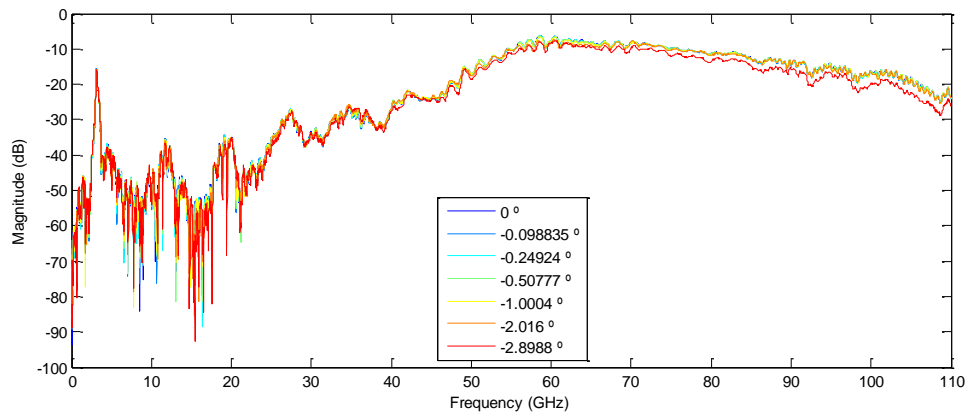
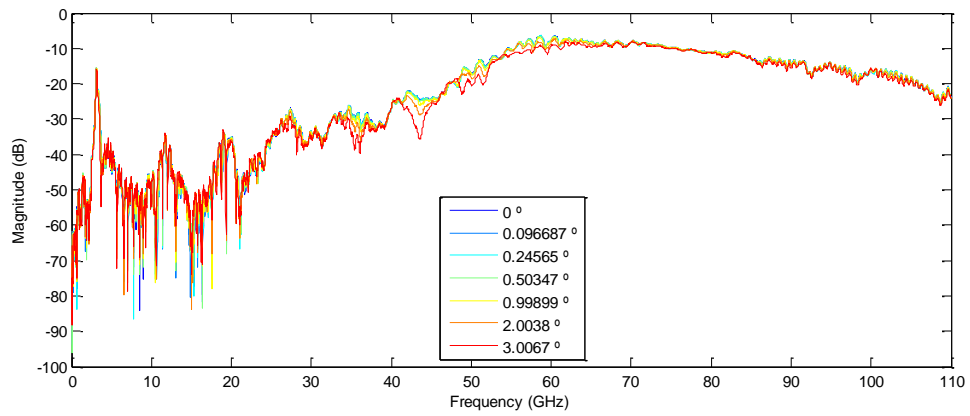


Figure A1-4. S21 at different yaw angles.

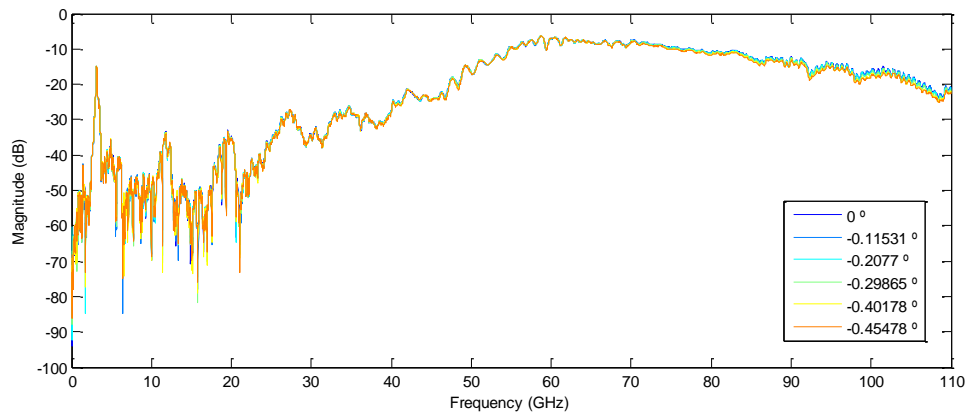
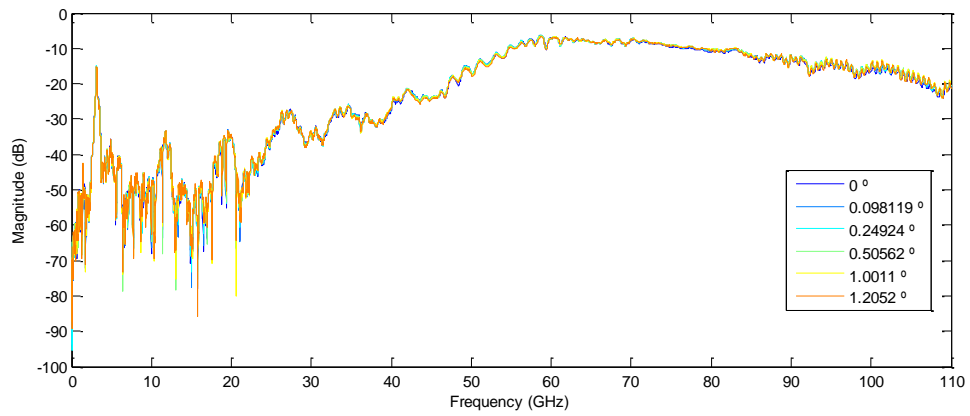


Figure A1-5. S21 at different pitch angles.